FEATURE ARTICLE

Size, Shape, and Structural Control of Metallic Nanocrystals

Isabelle Lisiecki

Laboratoire LM2N, UMR CNRS 7070, Université P. et M. Curie Bât F, 4 Place Jussieu, 75005 Paris, France

Received: January 13, 2005; In Final Form: April 6, 2005

In this review, we show that chemical reduction in colloidal assemblies favors the formation of size- and shape-controlled metallic nanoparticles. The key parameters that make possible the size control of spherical nanoparticles produced in spherical reverse micelles are the degree of hydration of the reactants, the dynamic character of the micelles, the capping with the surfactant, and the reducing agent concentration. The particle shape can be controlled by combining the strategy of the surfactant-based template and the capping of salts or molecules. Proof of the quality of the samples is given by the observation of two- and three-dimensional spontaneous self-organizations.

I. Introduction

Nanotechnology has been receiving increased attention in the past decade due to its extensive applications[1] in the field of catalysis, electronics, high-density magnetic recording media, sensors, and biotechnology. The challenge has been and remains the control of the size, the size distribution, and the shape of nanoparticles. The electrical, optical, and magnetic properties vary widely with these different parameters. Several approaches to produce the nanomaterials have been undertaken in the past decade.[2−16] In chemistry, two main methods have been employed to this end: coprecipitation and chemical reduction. In both cases, the presence of surfactant is required to govern the growth process. Typically, the coprecipitation reactions involve the thermal decomposition of organometallic precursors.[4,16−20] For instance, an organometallic precursor that rapidly decomposes gives rise to nanoparticles whose size is determined by the ratio of surfactant to precursor, whereas the shape is controlled by the specific adsorption of the surfactant used to modulate the relative growth rates of crystal faces. Moreover, the reaction has to occur at a given temperature and has to be quenched at a precise time in order to obtain the required nanocrystal. The chemical reduction occurring in colloidal assemblies is another approach for the formation of size- and shape-controlled nanoparticles.[6,7,21,22] Nevertheless, the mechanisms monitoring these controls are partially different from that presented above. The shape of the nanoparticles is partially governed by the shape of the template. When the reaction takes place in spherical reverse micelles, most of the nanoparticles are spherical. Some discrepancies are observed,[21] but for metallic (Ag, Cu, etc.)[6] and semiconductor (Ag_2S, CdS, CdMnS, and CdMnSe) nanoparticles,[23] this trend is verified. The size of spherical nanoparticles is controlled by the use of functionalized reverse micelles where the counterion of the surfactant is a reactive agent. Under these conditions, one of the key parameters involved in the nucleation process is the degree of hydration of the reactant, that is, the micellar size that can be well controlled. Otherwise, the intermicellar interactions, the capping with surfactant, and the reducing agent concentration govern the growth processes. As for the shape, it can be controlled by using nonspherical templates. In this way, elongated copper nanocrystals can be obtained when the synthesis takes place in cylindrical reverse micelles[24] or in an interconnected cylinder phase.[25] Nevertheless, the mimicry related to the shape is not optimal. By combining the strategy of the surfactant-based template with the capping involving salts or specific molecules, it appears that the particle shape can be more efficiently controlled.[26−27] Now, as pointed out above, nonspherical shapes can also be obtained in spherical reverse micelles. For instance, this is the case for tetrahedral cadmium sulfide[28] trigonal lamellar silver[30] and copper[31] nanocrystals. It is interesting to note that, in these cases, the synthesis takes place in a large excess either of reducing agent or of one of the reagents.

Therefore, it appears that if the control of particle size is almost well understood, this is not the case for the shape control. For any synthesis approach, very few reports are related to the control of particle shape; therefore, it is still rather difficult to determine the key parameters. Many parameters have to be taken into account, and an additional difficulty lies in the fact that the fabrication of a given nanomaterial is uniquely related to its physical and chemical properties.

Another present challenge is to order nanocrystals in 2D and 3D arrays on a macroscopic scale. These superlattices provide a new horizon in fundamental physics and are used as model systems for considering phenomena related to dipolar interactions within the solid. The first 2D and 3D superlattices were observed with Ag_2S and CdSe nanocrystals.[32,33] Since then, several groups have concentrated their efforts on producing self-organized lattices of, for instance, silver,[34−41] cobalt,[42−46] and alloys as NiFe.[47] Upon depositing these nanocrystals on a surface, collective optical[48,49] or magnetic[43,46,50−54] properties due to long-range dipolar interactions are observed.

In this paper, we describe the size and shape control of copper nanocrystals synthesized by chemical reduction in colloidal assemblies used as templates. We discuss the various parameters involved in the nucleation and growth processes. For spherical cobalt nanocrystals, we give evidence of their quality through

10.1021/jp058018p CCC: $30.25
Published on Web 06/08/2005

their ability to self-organize in 2D and 3D arrays. Let us first briefly describe the colloidal systems used here and their properties.

II. Reverse Micelles

II.1. Reverse Micelles Made of Monovalent AOT Surfactant. Surfactants are molecules with a polar hydrophilic head (attracted by water) and a hydrophobic hydrocarbon chain (attracted by oil). If the surfactant has the shape of a champagne cork (small polar head and branched hydrocarbon chains) spherical water-in-oil droplets are formed. These are usually called reverse micelles.[55] They are a thermodynamically stable mixture of water, oil, and surfactant where the water and oil regions are separated by a surfactant monolayer. Due to the amphiphilic nature of the surfactant, numerous disordered or partially ordered phases are formed depending on temperature and concentration.[56] The surfactant most used is sodium di(2-ethylhexyl) sulfosuccinate, usually called Na(AOT). The water/isooctane/Na(AOT) ternary phase diagram shows a large zone where the reverse micellar phase is found. In this liquidlike phase, the ratio of water to surfactant concentration, $w = [H_2O]/[Na(AOT)]$, determines the reverse micelle size. At w values below 15, water mobility is greatly reduced (bound water). Above $w = 15$, the linear increase in the water pool diameter, d_w, with w (from 6 to 18 nm) is explained by a geometrical model[57] that assumes a constant area per surfactant molecule and that all surfactant molecules participate in the reverse micelle interface. They are able to exchange their water contents during collision between two droplets. The volume of water added to the solution is the only parameter controlling the droplet diameter. Hence, the droplet size remains unchanged in various bulk oil solvents. The intermicellar potential, modeled by an adhesive sphere potential, depends on the particle diameter, d, the attractive range, D, and the sticky parameter, t^{-1}, describing the attractive strength between two droplets.[58] The latter increases with the length of the bulk oil alkyl chain. It is related to the decrease in percolation threshold with oil chain length and is explained in terms of an increase in intermicellar droplet interactions. This is due to penetration of solvent molecules in the interface screening the AOT alkyl chain interactions. In the case of long-chain oil solvents, steric hindrance does not allow solvent molecules to penetrate the interface, inducing an increase in the attractive interactions.[59−62] The kinetic exchange process[63] is directly related to the sticky parameter and to the binding modulus of the film at the water−oil interface. The solvent used tunes the kinetic exchange process: for short-chain solvents, the surfactant alkyl chain is well solvated and the micellar interactions are weak, inducing a low kinetic exchange rate constant. Conversely, large molecules are poor solvents for the alkyl chains, inducing strong interactions between micelles, that is, high kinetic rate constants. Hence, by replacing cyclohexane by isooctane as the bulk oil solvent, the kinetic rate constant, at fixed droplet size, increases by a factor of 10.[63] The kinetic exchange process is also tuned by the polar volume fraction. Indeed, from small-angle X-ray scattering (SAXS) measurements, using the Baxter potential, the sticky parameter of AOT reverse micelles, at a given water content, is found to decrease with the polar volume fraction.[64]

These two properties, size and exchange process, make it possible, by mixing two micellar solutions containing the reactants, to produce nanomaterials.

II.2. Colloidal Self-Assemblies Made of Divalent AOT Surfactant. Following our paper[65] in 1991, a great deal of work has been done with divalent bis(2-ethylhexyl) sulfosuccinate, $X(AOT)_2$. We demonstrated that, at low water content, spherical reverse micelles are formed. In the case of $Cu(AOT)_2$, $Co(AOT)_2$, and $Cd(AOT)_2$, upon an increase in the water content, spherical water-in-oil droplets turn into cylinders. This study has been extended by other groups: Eastoe et al.[66−69] confirmed these data and showed this for other surfactants such as $Zn(AOT)_2$, $Ni(AOT)_2$, and $(C_7H_{14})_4N(AOT)_2$.

In the oil-rich region, the phase behavior of copper(II) bis(2-ethylhexyl)sulfosuccinate, $Cu(AOT)_2$−isooctane−water, is known over a wide domain.[25,70−73] The system exhibits an extraordinary diverse range of phases depending on the water content (Figure 1). When the surfactant is not totally solvated, $w \leq 15$, the various structures are governed by the hydration of the head polar group with a progressive increase in the surfactant parameter, $s = v_s/a_s l_s$, where v_s, a_s, and l_s are the volume of the surfactant, the surface area, and the length of the alkyl chain, respectively. As a consequence, a change in their curvature occurs.

(i) At low water content, below $w = 5$, a homogeneous reverse micellar solution (the L_2 phase) is formed. In this range, the shape of water droplets changes from spheres (below $w = 4$) to cylinders. At $w = 4$, their width and length, determined by SAXS, are 2.4 and 4 nm, respectively.

(ii) Upon an increase in the water content ($5 < w < 9$), a phase transition takes place with the formation of interconnected cylinders (the L_2* phase) with a width of 3 nm.

(iii) A further increase in the water content induces the appearance of an additional phase (the L_α phase) composed of a mixture of planar lamellae and spherulite lamella-like phases. While the existence of this region is quite limited, $9 < w < 10$, it is nevertheless of great interest with respect to the shape control of copper nanocrystals (see section V.1).

(iv) At $w = 10$, there remains only the L_α phase, mostly composed of planar lamellae. This phase remains stable up to $w = 15.5$, and at this point of the phase diagram, all of the surfactant is solvated.

Hence, the progressive solvation of the surfactant is accompanied by a regular change of the structure curvature from the spheres to the planar lamellae. Let us now consider the other structures formed by further increasing the water content.

(v) At $w = 15.5$, an isotropic phase appears in equilibrium with a spherulite phase. Upon an increase in the water content from 15.5 to 26, the former progressively increases, whereas the latter disappears. This behavior is related to the transformation of spherulites which do not remain stable. With increasing w, they progressively collapse and thus release surfactant that reorganizes into an interconnected phase. At this stage, the spherulites become a complex system containing and surrounded by an interconnected cylinder phase; they are called "supra"-aggregates. From a theoretical model based on geometry and energetic considerations,[74] the spherulite interior has to collapse to form interconnected cylinders. With a further increase in water content, the interior (highly curved) bilayers become energetically unfavorable as more and more oil is exposed to the water interface.

(vi) An increase in the water content from $w = 26$ to $w = 28.5$ causes the complete disappearance of the spherulite phase. The remaining isotropic phase is attributed to the L_2* phase similar to that obtained at lower water content ($5 < w < 9$).

(vii) Upon an increase in w above $w = 28.5$, the isooctane phase progressively disappears until one isotropic phase is reached. Below $w = 32$, interconnected cylinders are formed and progressively transform into isolated spheres ($w > 32$). At this stage, the headgroup is fully hydrated and curvature at the interface remains constant. With increasing water content, the

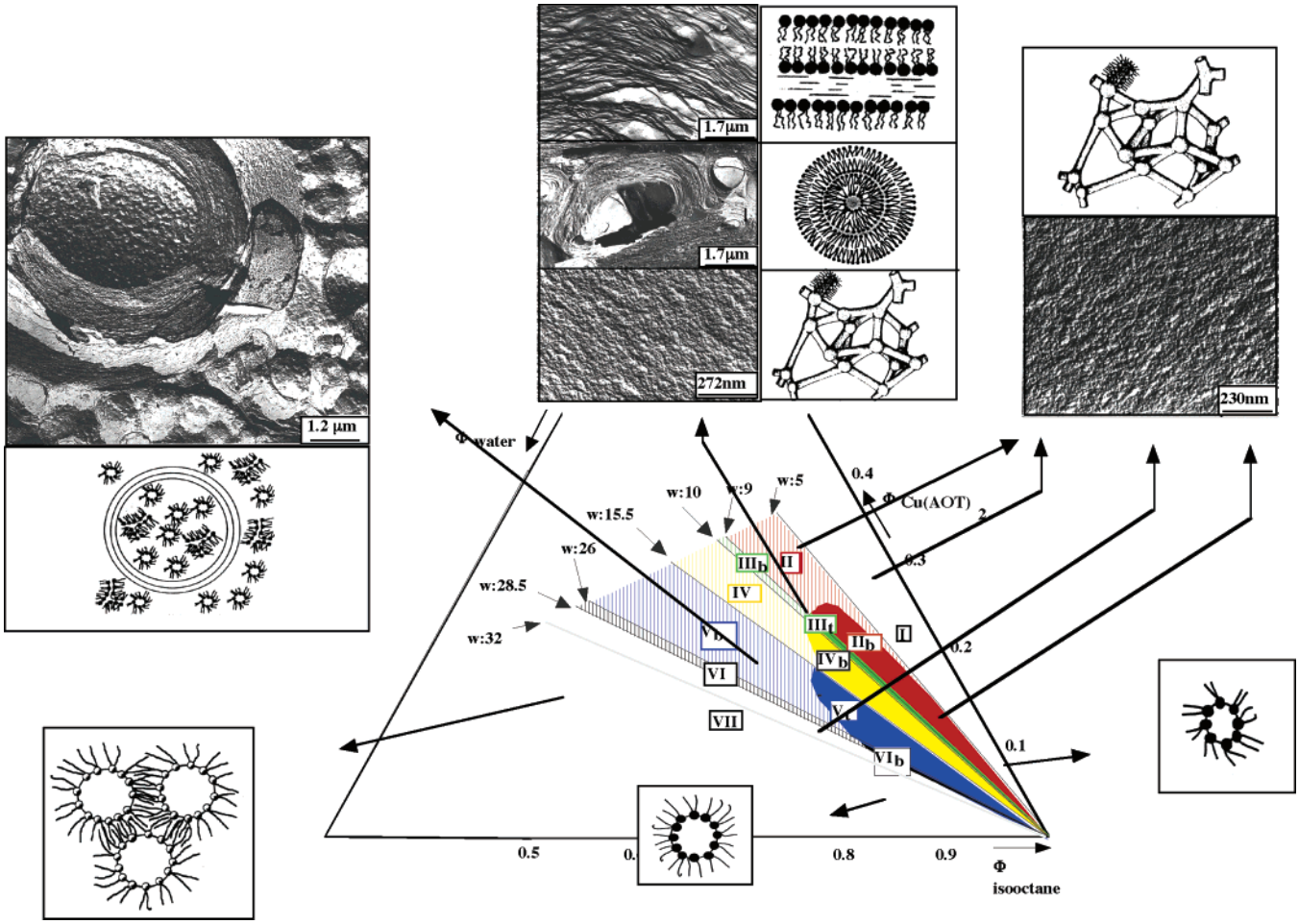

Figure 1. Phase diagram of $Cu(AOT)_2$/water/isooctane in the oil-rich region.

only solution to the problem of maintaining constant average curvature consistent with global packing is achieved by reducing connections in the network which ultimately becomes disconnected spheres. The mean diameter of the spheres is 6 nm, while the mean width and length of the cylinders are 11 and 15 nm, respectively. At high surfactant concentration, because of a lack of solvent, clumps of interdigitated micelles form.

It must be noted that the phase boundaries of such a diagram emerge qualitatively from elementary considerations that require only notions of local and global packing constraints.[75]

Reverse micelles can be either mixed or pure:

(i) A mixed micellar system is one where only a part of the surfactant is functionalized while the rest is the sodium derivative. When about 20% (and less) of the surfactant is functionalized, spherical reverse micelles are formed whose size increases with the water content, as is the case of the Na(AOT)/water/solvent solution. With an increase in w from 1 to 15, the hydration state of the metallic counterion is progressively increased. Regardless of the chemical reduction that will occur in this environment, it is clear that the ability of the system to vary its hydration state constitutes an efficient way to control the nucleation and growth processes of the nanocrystals.

(ii) A pure micellar system is entirely made of divalent metallic counterions. In contrast to the mixed system, pure reverse micelles are most useful for working at very high concentrations of reagents. Indeed, the number of reactive ions in the micelle is optimal, that is, one ion per two AOT surfactant molecules. It must be noted that whether the divalent counterion is Cu^{2+} or Co^{2+}, the ternary phase diagram of this system does not change.

III. Size Control by Various Parameters of Spherical Copper Nanocrystals[76,77]

Copper nanocrystals are made in mixed reverse micelles. Experimental details can be found in Appendix A.

III.1. Role of the Water Content. The size of copper nanocrystals produced by procedure A1 varies with the water content (Figure 2). The corresponding average diameters are given in Figure 3.

With an increase in the w value, inhomogeneous size changes are observed. From $w = 1$ to $w = 5$, the mean diameter of nanocrystals significantly increases from 2.1 to 9.5 nm. Above $w = 5$, the growth rate drastically decreases. At $w = 10$, the mean diameter reaches 12.6 nm, and despite the further increase in w, it finally stays constant. We recall here that the micellar diameter increases from around 2 nm to 6 nm when w increases from 1 to 15. Thus, it clearly appears that, whatever the w value, the sizes of the copper nanocrystals are always larger than those of the micelles (Figure 3). Furthermore, the increase in the production of Cu nanocrystals varies. At low w, nanocrystals are very sparse on the carbon film, while their density increases with increasing w values. This fact is partly confirmed by the increase in the plasmon peak intensity at high w values, while the sizes stay almost constant.[77]

Similar size behavior with, nevertheless, some discrepancies has been observed with other nanomaterials such as semiconductors[23] and metals.[78] In most cases, the size of the produced nanomaterial, under the same experimental conditions, is not that of the micelles. In addition, a limited nanocrystal size is always reached at a w value around 10−15. This maximum

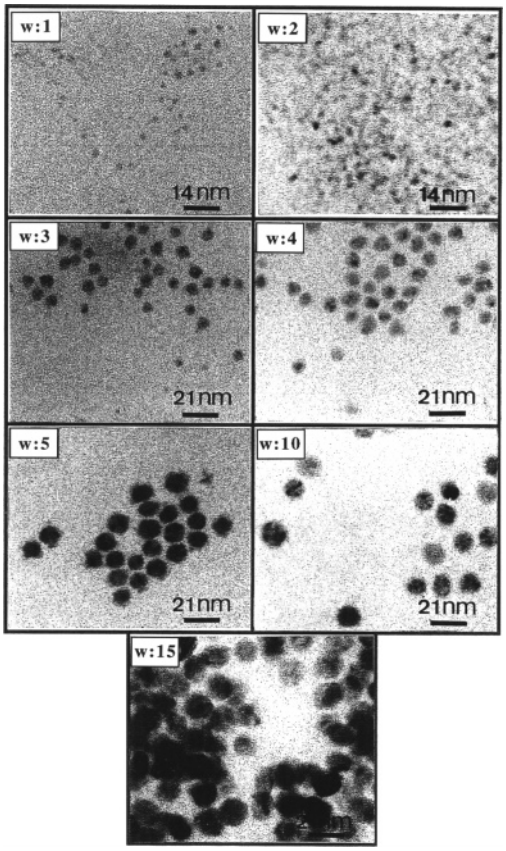

Figure 2. TEM patterns of copper nanocrystals synthesized in mixed AOT reverse micelles at various water contents, *w*.

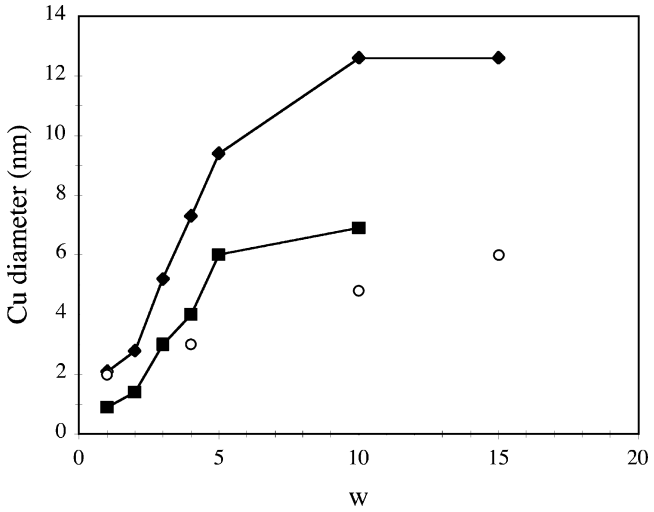

Figure 3. Variation of the mean diameter of copper nanocrystals synthesized in mixed AOT reverse micelles at various water contents, *w*. The solvents are (◆) isooctane and (■) cyclohexane. This variation can be compared with that of the diameter of (○) AOT reverse micelles with the *w* value.

size varies with the material: for semiconductors such as CdS, CdTe, and CdMnS, it is around 4 nm, whereas, for metals such as silver, it is around 7 nm.

The increase in size is attributed to a change in the structure of water,[79] that is, the hydration of metallic ions. At very low *w* values, the reactants are poorly hydrated and the yield of the reduction or coprecipitation reactions is very low. Such a reaction gives rise to small nanocrystals. Conversely, the increase in the reactant hydration induces the increase in the yield of the reaction, so that the number of nuclei increases. Then, the size (and production for, at least, the case of copper) of nanocrystals increases. By assuming that all of the system is totally hydrated at $w = 15$, whatever the material, the nanocrystal growth should evolve up to $w = 15$ and then stop. Now, this is not the case. For copper, the production of nanocrystals increases well up to $w = 15$ but their growth starts to decrease at $w = 5$ and finally stops at $w = 10$. In the same way, the limited *w* value related to the other materials is not a constant but is typical of the material. Such discrepancies can be partly attributed to capping with the AOT surfactant molecules. While there is now no doubt that surfactant adsorbs at the nanomaterial surface, the question that still arises is the following: At which stage does it limit the nanocrystal growth? Regardless of all the above data, it is clear that this fact mainly depends on the synthesized material, that is, the affinity of the surfactant with the material. When the AOT/nanomaterial affinity is low, a rapid growth with *w* value can be expected, a growth that is mostly governed by the hydration state of the reagents. This is the case, for example, for copper with a maximum diameter relatively large compared to the others, around 12 nm. The low affinity of the surfactant with the metal is further confirmed by the fact that copper nanocrystals are always much larger than the micelles (there is a factor of about 2). The AOT adsorption at the copper surface is not efficient enough to limit the nanomaterial growth even when the nanocrystal size becomes similar to and then larger than that of the micelles. It becomes efficient when the nanocrystal size is twice that of the micelle. Conversely, when the AOT/nanomaterial affinity is high enough, the nanocrystal growth is expected to be lower compared to the previous case. Under these conditions, AOT surfactant is assumed to adsorb at the nanocrystal surface, earlier, during the growth process. This means below or when the nanocrystal size reaches that of the micelles. This is the case for the group of semiconductors (CdS, CdTe, and CdMnS) and silver nanocrystals characterized by limited sizes, 4 and 7 nm, respectively. Nevertheless, the fact that the reaction schemes differ with the synthesized material can also contribute to influencing the growth process, that is, to induce various limited sizes.

III.2. Role of the Interactions between Reverse Micelles. As reverse micelles constitute a dynamic system, they also make possible, through the interactions between droplets, control of the nanocrystal growth. Thus, changing either the bulk solvent used to form the reverse micellar solution or the polar volume fraction modifies the intermicellar exchange process.[77]

By replacing isooctane with cyclohexane as the bulk solvent (see procedure A2), we observe that, whatever the *w* value, copper nanocrystal diameters are lower than those obtained when the solvent is isooctane (Figure 3). The mean diameter increases from 1 to 6 nm when *w* increases from 1 to 15. In addition, it must be noted that the curves obtained for both solvents are similar; that is, the growth rate decreases from $w = 5$ toward a limited value. The size decrease recorded when the solvent changes from isooctane to cyclohexane well illustrates the fact that the kinetic exchange process decreases through the decrease in the sticky parameter. Indeed, the decrease in the solvent molecule volume induces an increase in the attractive interactions between micelles (see section II.1). Now, it can be assumed that the nucleation process of copper nanocrystals mostly takes place inside a given micelle. Nevertheless, the growth of the copper seeds so produced is directly related to the exchange of the water pools between two micelles occurring during the exchange process. During this exchange, copper seeds grow by attracting either isolated copper atoms or other metallic seeds initially formed in a neighboring micelle. Consequently, de-

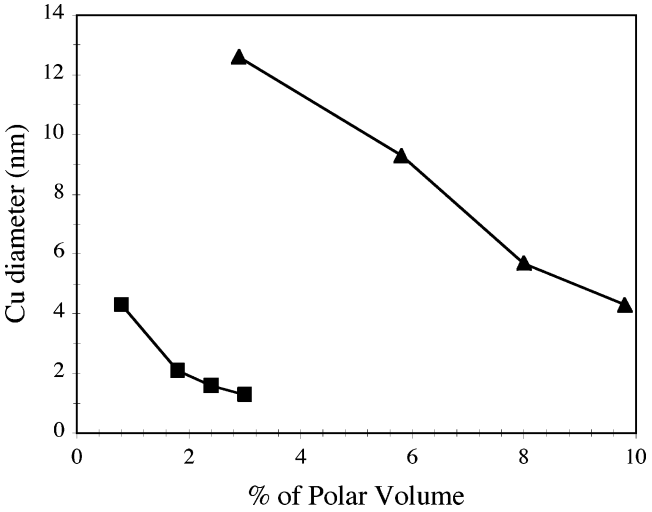

Figure 4. Variation of the mean diameter of copper nanocrystals synthesized in mixed AOT reverse micelles with the polar volume fraction: $w =$ (■) 3 and (▲) 10.

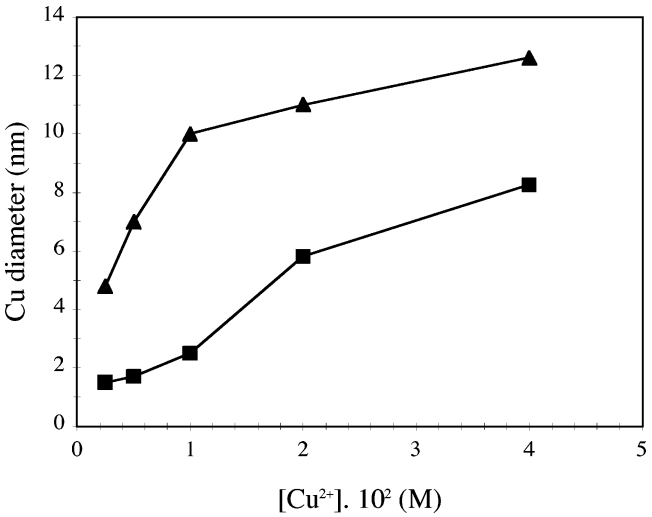

Figure 5. Variation of the mean diameter of copper nanocrystals synthesized in mixed AOT reverse micelles with overall copper ion concentration: $w =$ (■) 3 and (▲) 10.

creasing the kinetic exchange process induces a decrease in the nanocrystal growth rate. In the present case, because the micellar size does not change with the nature of the solvent, the exchange process is the only parameter that can tune the nanocrystal size. Nevertheless, it cannot be excluded that there is a higher efficiency of the AOT capping that would be favored by the enhancement of the intermicellar exchange process. This fact could explain the decreasing growth rate observed from $w = 5$ while the nanocrystal size is only around 6 nm.

The polar volume fraction is changed by changing the micellar concentration in the solution (see procedure A3). In this case, the ratio of the copper AOT concentration to the sodium AOT concentration stays the same. Hence, at fixed w, the average number of copper ions per micelle remains constant. However, the increase in the polar volume fraction induces both the increase in the overall concentration of copper ions and the increase in the micellar exchange rate. Let us consider the role of the overall concentration of the reactive copper ions. By increasing the copper AOT concentration (see procedure A4), Figure 5 shows, for various water contents ($w = 3$ and 10), the increase in the nanocrystal size. This behavior is related both to the local and to the overall reactive ion concentration increases. Indeed, when reactive ions locally concentrate inside

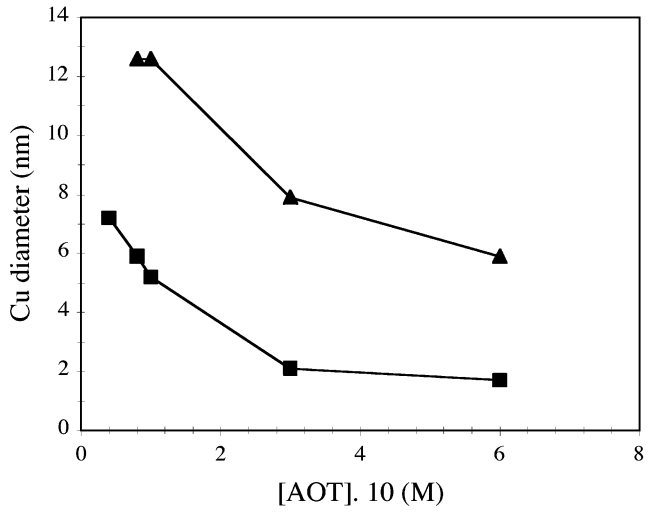

Figure 6. Variation of the mean diameter of copper nanocrystals synthesized in mixed AOT reverse micelles with overall AOT surfactant concentration: $w =$ (■) 3 and (▲) 10.

the micelle (whose size stays the same), the nucleation process induces the formation of larger seeds for which subsequent growth will give rise to larger nanocrystals. Now, the increase in the overall reactive ions in the solution plays a role in the growth process; the latter is enhanced because of the higher concentration of copper seeds present in the solution. Thus, the increase in the polar volume fraction induces two opposite size behaviors: through the increase in the overall concentration of copper ions, we favor the increase in the growth of the copper seeds, whereas the decrease in the micellar exchange rate acts exactly in the opposite way. In fact, Figure 4 clearly shows that, whatever the water content ($w = 3$ and 10), the nanocrystal size significantly decreases. This clearly shows that the growth of the copper seeds is here governed more by the micellar exchange process than by the overall copper ion concentration.

From these data, it is clear that the intermicellar exchange process directly related to the growth process of the copper seeds can also contribute to controlling the growth of copper nanocrystals whose size increases with the efficiency of the exchange process. Nevertheless, it also cannot be excluded that there is a higher efficiency of the AOT capping that would be induced by the intermicellar exchange rate increase.

III.3. Role of AOT Capping. The overall AOT surfactant concentration increases by increasing that of sodium AOT (see procedure A5). Nevertheless, by increasing the sodium AOT concentration and by keeping that of the copper AOT constant, three effects have to be taken into account.[77] The first is the higher efficiency of the AOT capping effect due to the increase in the ratio of the sodium AOT concentration to the copper AOT concentration. The second is the decrease in the intermicellar exchange rate due to the increase in micellar concentration, that is, the polar volume fraction. The third is the decrease in the local concentration of copper ions per micelle. In fact, as it has been well demonstrated in the cases presented below, all these effects play a role during the growth process and act in the same way. They limit the growth of the copper seeds, and the final nanocrystal sizes thus obtained decrease. This fact is well illustrated in Figure 6 showing, that at $w = 3$ and 10, the mean diameter significantly decreases with the AOT surfactant concentration from 7.2 to 1.5 nm and from 12.6 to 6.2 nm, respectively.

From all these results, it is clear that AOT reverse micelles constitute good nanoreactors for synthesizing spherical metallic

TABLE 1: Average Diameter of Cobalt Nanocrystals, *D*, and Size Distribution, σ, at Various *R* Values

R	0.5	1	2	4	6	8
D (nm)	6	7	7	7	7	8
σ (%)	30	18	13	12	12	8

nanocrystals. Thorough knowledge of this complex system related to the reagent hydration, the intermicellar interaction, and the surfactant capping allows one to control the nanocrystal size by different ways.

IV. Size Control of Spherical Cobalt Nanocrystals. Toward the 2D and 3D Self-Organizations[80−82]

IV.1. Role of the Reducing Agent Concentration.[80] From the above considerations, AOT reverse micelles are good candidates for use as nanoreactors. However, AOT surfactant molecules can also be used as "simple" capping and stabilizing agents as in the organometallic precursor decomposition reactions. Indeed, in the case of cobalt synthesis, when they are made in a supersaturated regime, that is, at a high reducing agent concentration, reverse micelles are destroyed immediately after adding the reducing agent solution because of the limited water content.[80] In this way, the nucleation and growth processes take place in a poorly defined "macroemulsion". The choice of the supersaturated regime is here dictated by the need for magnetic nanocrystals characterized by both large size and low size polydispersity. The reducing agent used is sodium tetrahydroborate, and its concentration is represented by *R*, $R = [NaBH_4]/[Co(AOT)_2]$. Nanocrystals are synthesized at various *R* values as described in Appendix B. At $R = 0.5$, the average size is 6 nm, with a rather large size distribution of the nanocrystals, σ, of 30% (Table 1). This is in good agreement with previously published data.[83,84] When *R* increases from 0.5 to 8, two main behaviors are observed: (i) The mean diameter of cobalt nanocrystals increases from 6 to 8 nm. This is directly related to the increase in the yield of the reduction reaction that is not complete below $R = 8$. The concentration of the nuclei formed increases, and their subsequent growth induces larger and larger particles. This has to be compared with the increase in the copper ions in reverse micelles (see section III.2). (ii) The more important feature is the drastic decrease in the size distribution from 30 to 8%. This behavior is due to the size increase combined with the size selection that occurs at the end of the particle preparation, leading to the collection of the smaller nanocrystals. For any reducing agent concentration, magnetic measurements indicate the formation of metallic cobalt. They are characterized by poor face-centered cubic (fcc) crystallinity.

IV.2. 2D and 3D Self-Organizations of Cobalt Nanocrystals.[80−82] Let us now consider the transmission electron microscopy (TEM) images obtained at various *R* values, after the deposition and evaporation of 10 drops (10×10 μL) of a highly concentrated cobalt solution on amorphous carbon (Figure 7). The assemblies, obtained for $\sigma \leq 13\%$, clearly show that lauric acid-coated cobalt nanocrystals spontaneously organize into 2D hexagonal compact networks over longer and longer distances with increasing *R* (Figure 7C−F). At $R = 6$, the interparticle gap is around 2.5 nm. The length of the lauric acid chain in the all-trans conformation, 1.77 nm, indicates a partial interdigitation (around 1 nm) between chains used to passivate the nanocrystals.

To build 3D ordered superlattices, a larger volume of cobalt nanocrystal solution ($R = 6$) (20×10 μL) is deposited on highly oriented pyrolitic graphite (HOPG) substrate. After the solvent evaporation, the Co nanocrystals self-organize into a regular 3D superlattice, as shown in Figure 8. Their thickness can be

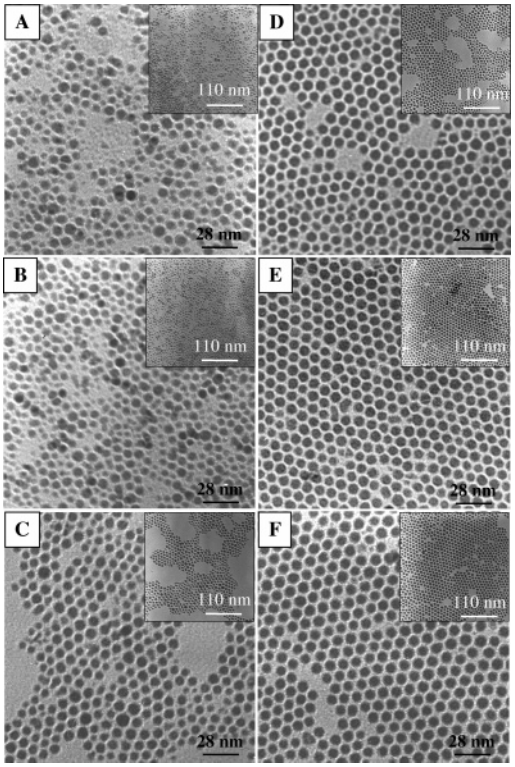

Figure 7. TEM patterns of cobalt nanocrystals synthesized in pure reverse micelles at various reducing agent concentration ratios, *R*: (A) $R = 0.5$; (B) $R = 1$; (C) $R = 2$; (D) $R = 4$; (E) $R = 6$; (F) $R = 8$.

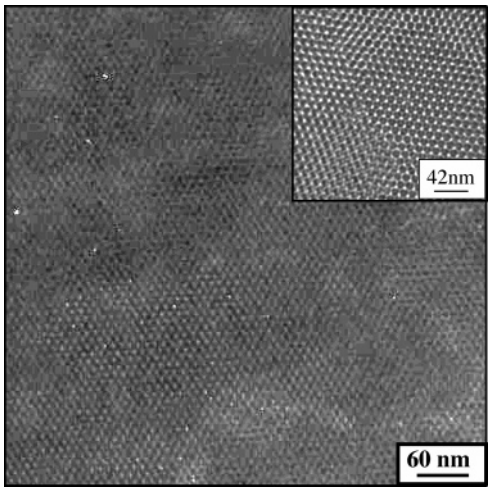

Figure 8. TEM pattern of a 3D superlattice of 7.2 nm cobalt nanocrystals obtained on HOPG substrate. Inset: higher magnification TEM image.

increased by horizontally immersing a HOPG substrate in 200 μL of the concentrated nanocrystal solution. Solvent evaporation takes place under a pure nitrogen flow, and the substrate temperature is maintained at 25 °C. The scanning electron microscopy (SEM) image in Figure 9A shows a film consisting of isolated domains that are relatively large, several thousand square micrometers, and separated by an average distance of 3 μm. Their thickness is about 5 μm (Figure 9B), and it must be noted that most of the deposition occurs at the border of the substrate. The cracking behavior giving rise to sharp edges is the result of surface tension stresses arising during evaporation. The X-ray diffraction pattern (inset of Figure 9C) shows the first and the second orders of Bragg reflections. The reflection width is nearly resolution-limited (0.03 nm^{-1}), indicating long-range ordering of the magnetic nanocrystals out of the substrate

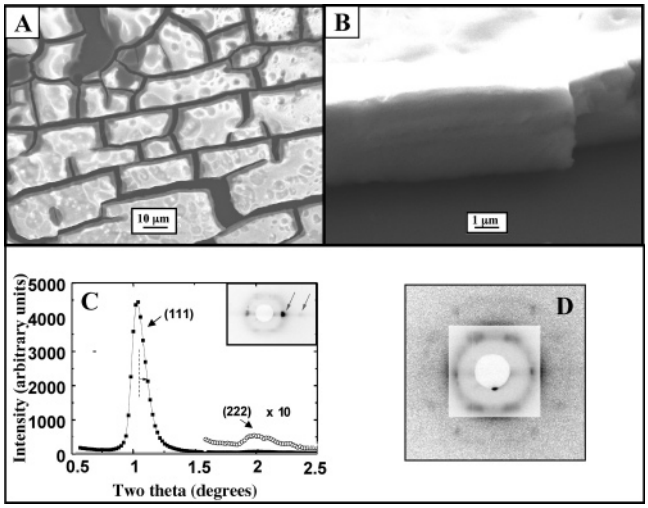

Figure 9. (A and B) SEM patterns of supracrystals of 7.2 nm cobalt nanocrystals obtained in a nitrogen atmosphere. (C) The $\Theta-2\Theta$ diffractogram and in the inset the corresponding X-ray diffraction pattern. (D) The X-ray diffraction pattern (tilt angle of substrate surface with respect to the incoming beam of 10°).

(Figure 9C). The stacking periodicity is 8.54 ± 0.05 nm. To probe the other planes, the sample is tilted by around 10°. Figure 9D shows nine additional Bragg reflections. These additional spots indicate a face-centered cubic (fcc), 3D long-range ordering within the nanocrystal domains. The observation of well-defined Bragg reflections is proof that the ordered domains share a common crystallographic normal-to-the-substrate axis. It can be further assumed that their in-plane orientation is random. This fact is partly explained by the various orientations of the domains on the substrate. It is important to note that such supracrystals made with several thousand Co monolayers remain stable with the same large-scale ordering for several months.

From these results, it can be concluded that the stabilizing role of the AOT surfactant combined with a size selection also allows the control of both the size and the size polydispersity of the cobalt nanocrystals. Such an accurate control makes possible the spontaneous formation of 2D and 3D magnetic arrays organized on a large scale and stable for several months.

V. Shape Control of Copper Nanocrystals

V.1. Shape Control by Using Colloidal Assemblies. Copper nanocrystals are synthesized in various regions of the phase diagram isooctane/Cu(AOT)$_2$/water, as described in Appendix C. The objective is to carry out Cu syntheses in the various microstructures (reverse micelles, interconnected cylinders, supra-aggregates, etc.) to determine if there is a change in the particle morphology. The results, shown in Figure 10, are the following:[25]

(i) In the presence of isolated reverse micelles, below $w = 5$ and above $w = 32$, most of the copper particles are spherical. In weight percentage, only 13% of copper particles are cylinders. The particle dimensions are lower at higher w. The average diameter of spheres decreases from 12 to 7.5 nm, whereas the width and length of cylinders decreases from 18.5 to 8.2 nm and 12 to 6.6 nm, respectively. Now, when spherical reverse micelles are interdigitated, at high surfactant concentrations and above $w = 32$, spherical nanocrystals with a very low size polydispersity and a mean diameter of 7.5 nm self-organize into 3D arrays.

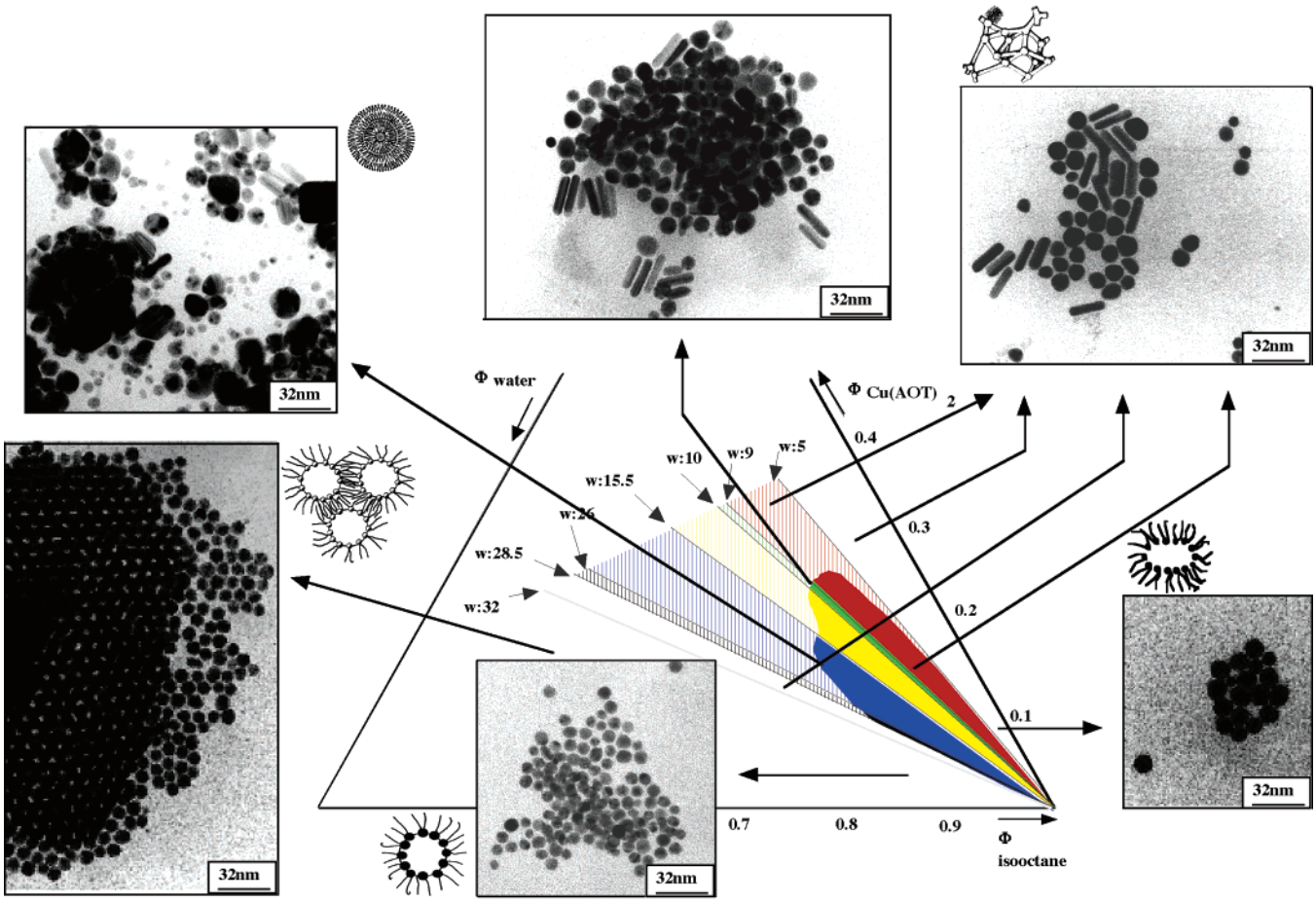

Figure 10. Various shapes of copper nanocrystals made in the various parts of the phase diagram shown in Figure 1.

(ii) Interconnected cylinders having similar persistence lengths are formed in two water content ranges ($5 < w < 9$ and $28.5 < w < 32$). Syntheses in these two domains show very strong correlations and similar data. Spherical and elongated particles are formed in both cases. In both domains, the average diameter of spherical particles is the same, 9.5 nm. Similarly, the size of the elongated particles remains identical with an average length and width of 21.2 and 6.6 nm, respectively. In weight percentage, about 50% of copper particles are elongated.

(iii) When syntheses take place in the presence of a mixture of an interconnected cylinder phase and the L_α phase containing both spherulites and planar lamellae ($9 < w < 10$), the weight percentage of elongated particles remains about 50%. Their average length and width are 24 and 8 nm, respectively. The rest of the population is mainly spheres with a few percent of other shapes such as squares and triangles.

(iv) In the presence of supra-aggregates made of spherulites containing in their interior and surrounded by an interconnected cylinder phase, the syntheses produce particles having a much higher polydispersity in size and shape than those found at other water contents. Triangles, squares, spheres, and elongated particles are observed.

These results tend to show that the shape of the colloidal microreactor partially controls the shape of the nanocrystals. Indeed, spherical particles make up the main population obtained in reverse micelles, whereas elongated particles are mainly obtained when the synthesis takes place in the presence of an interconnected cylinder phase. We can note that the former synthesis is related to a dynamic system governed by the intermicellar interactions, whereas the latter occurs in a "quasi"-static system. Now, the shape of the particle is largely dependent on its crystallographic characteristics related to the core and the enclosed surfaces. From such a viewpoint, the particle shape can be determined by both (i) the structure of the copper precursor and (ii) the kinetics of particle growth that can be controlled by the specific adsorption of surfactant molecules or other molecules on the growing crystal. It must be noted that such a kinetic control is all the more required in that the material does not possess an intrinsic anisotropic structure. In addition, the chemical reaction has to occur in a medium that is sufficiently confined to induce high particle crystallinity.

The elongated copper nanocrystals observed in the present case are characterized by a truncated decahedral structure.[85,86] Indeed, this is well shown by comparing the high-resolution transmission electron microscopy (HRTEM) image of an elongated particle (Figure 11A) and the HRTEM simulated image of a truncated decahedron (Figure 11C). The calculated PS (Figure 11B) has three pairs of equatorial reflections labeled 1, 2, and 3 with sideband reflections labeled 4, 5, 6, 7, 8, and 9. These reflections correspond to the following lattice parameters: $d_1 = 0.128$ nm, $d_2 = 0.210$ nm, $d_3 = 0.338$ nm, $d_4 = d_9 = 0.181$ nm, $d_5 = d_8 = 0.217$ nm, and $d_6 = d_7 = 0.250$ nm. Reflections 1, 2, 4, and 9 correspond to the Cu(220), (111), (200), and (020) plane spacings, respectively (0.1278, 0.2087, 0.1808, and 0.1808 nm). The angle between (200) and (020) is 90°. The appearance of the (200) and (020) reflections together with the (111) reflection proves that the particle consists of two or more fcc subunits that must be twinned together. Reflections 3, 5, 6, 7, and 8 are caused by multiple scattering effects. This PS, that is similar to the simulated one (Figure 11D), clearly indicates a truncated decahedron. The formation of this structure is based on the regular decahedral precursor that is one of the precursors for metallic copper. It is made up of five deformed fcc tetrahedrals bounded by (111) planes. Its growth is accompanied by the progressive truncation of the five subunit edges, inducing the {100} lateral facets (Figure 11E). Hence, the particle growth is hindered and takes place in the [110] direction, that is, the 5-fold axis. Such a shape is determined from the preferential growth of the {111} facets compared to the growth of the {100} facets. This process is related to the selective adsorption of AOT surfactant on the lateral {100} facets.

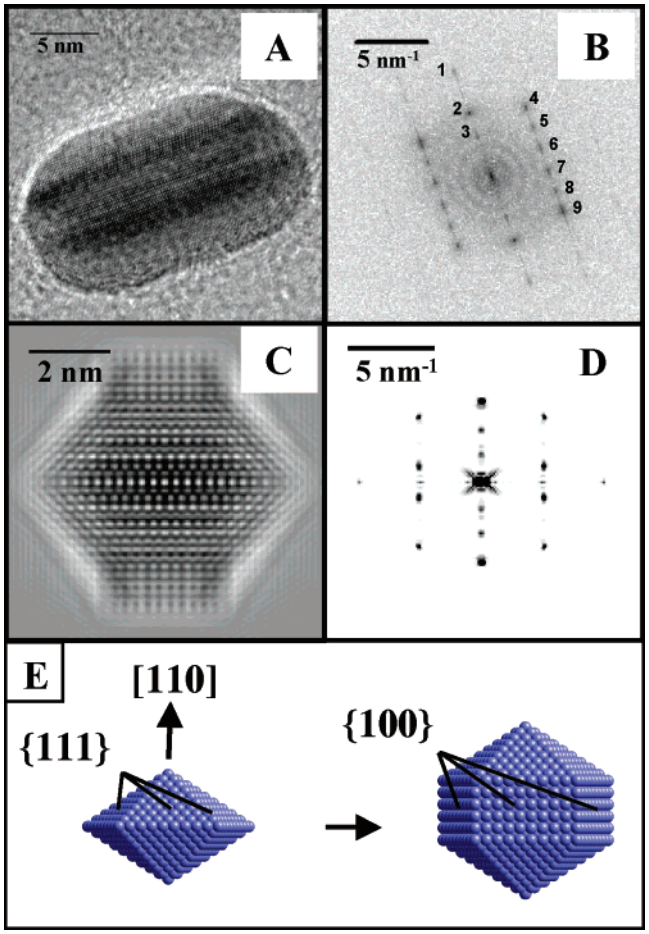

Figure 11. Elongated copper nanocrystals in the [001] orientation produced at $R = 15$: (A) HRTEM of a truncated decahedron; (B) power spectra in the [001] orientation; (C and D) computer simulation; (E) schematic of the growth mode of elongated nanocrystals.

Therefore, it appears that the formation of elongated copper nanocrystals requires both (i) the presence of a decahedral precursor and (ii) the preferential AOT adsorption in order to kinetically control the growth rates of the crystal facets. Clearly, such an adsorption is greatly favored in the presence of an interconnected cylinder phase. In fact, it is quite likely that the tubular shape of the microreactor favored, initially, the surfactant adsorption on the fcc subunit edges. Subsequently, the resulting {100} facets are preferentially adsorbed by the surfactant that induces the particle growth along the 5-fold axis of the multiplied twinning particle. Conversely, in the presence of spherical reverse micelles, the first step inducing the lateral facets is missed and the decahedral precursor growth is no longer uniaxial but mostly occurs homogeneously. In this case, AOT surfactants adsorb on the five {111} precursor facets, inducing the formation of pentagonal shapes, that is, of regular decahedral structures. Depending on their size and the possible presence of defects, these nanocrystals appear more or less spherical. From this, it is clear that the colloidal microreactor used to synthesize copper nanocrystals plays the role of a template. In

the literature, some examples tend to give evidence of the surfactant-based templates. Elongated CdS particles grow in cylindrical reverse micelles, while spheres are obtained in spherical reverse micelles.[87] PbS particles are formed in a Pb(AOT)$_2$/PVB polymer composite;[88] according to whether this has an ordered layer structure or not, nanorods or spherical particles are obtained. On the other hand, it also appears that particle crystallinity is enhanced when there is an interconnected cylindrical phase compared to the micellar phase. Indeed, spherical particles often have defects, whereas elongated particles are mostly highly crystallized. This can probably be attributed to the degree of confinement of the reagents that is much higher in the interconnected microstuctures than in the micellar system. In fact, reverse micelles are dynamic systems and the "real" confinement they offer compared to the interconnected cylinder phase is less. Therefore, this system gives rise to a higher percentage of polycrystals (compared to the interconnected cylinder phase), whose typical shape is the sphere.

From these results, it appears that the various key parameters involved in the formation of the elongated nanocrystals are the precursor structure, the confinement degree of the reactive medium, and the AOT capping related to both the shape of the template and the surfactant/{110} copper crystal facet affinity. Now, it must be noted that such a template effect remains partially related to the aspect ratio of the elongated nanocrystals and their population percentage.

V.2. Shape Control by Using Water-in-Oil Self-Assemblies in the Presence of Salts. As shown above, uniaxial growth of copper nanocrystals is related to specific AOT adsorption that mainly occurs in the presence of an interconnected cylinder phase. From this, other molecules such as salts have been tested in order to investigate their ability to control the growth rates of copper crystal facets. Hence, syntheses were carried out in the phase containing the interconnected cylinders with the L_α phase ($9 < w < 10$), in the presence of a small amount of a salt (see Appendix D). Various salts have been tested.[26,27]

Let us first consider the behavior observed with sodium chloride. The presence of this salt induces the formation of a population of nanocrystals having, as with no salt present, various shapes such as spheres, cubes, triangles, hexagons, pentagons, and elongated particles. The elongated nanocrystals always constitute the highest shape weight percentage, and depending on the salt concentration, their size can be tuned (Figure 12). The average length increases with the salt concentration from 24 to 300 nm and then decreases, whereas the average width continuously increases from 8 nm. The average aspect ratio is characterized by a maximum of 15 (Figure 13). By replacing NaCl by another chloride salt such as KCl, $CuCl_2$, or CTAC (cetyltrimethylammonium chloride), the recorded behaviors remain unchanged; that is, the highest shape weight percentage is that of the nanorods whose size can be similarly tuned by the salt concentration. These results clearly give evidence of the major role played by the chloride anion during the growth process of elongated copper nanocrystals. This is further confirmed by the fact that the use of NaF or NaI, for instance, does not induce any change in the nanocrystal shape compared to the syntheses made in the absence of salt. From an initial viewpoint, this shape behavior cannot be attributed to changes in the microemulsion structure. In fact, the structural study of the template shows only a very slight change upon the salt addition.[89] The control of the nanocrystal shape is explained in terms of selective adsorption with chloride anions. Like the AOT surfactant molecules, Cl^- anions selectively adsorb on the

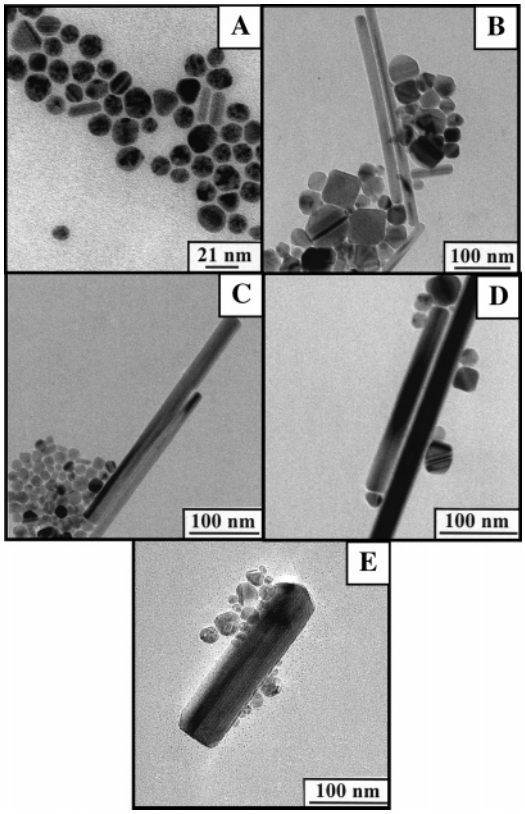

Figure 12. TEM patterns of copper nanocrystals obtained in the interconnected cylinder phase in the presence of sodium chloride: (A) [NaCl] = 0; (B) [NaCl] = 5×10^{-4} M; (C) [NaCl] = 1.1×10^{-3} M; (D) [NaCl] = 1.6×10^{-3} M; (E) [NaCl] = 2.2×10^{-3} M.

lateral {100} facets of the growing truncated decahedron (see section V.1), but it is clear that such a capping much more efficiently retards the growth of the {100} facets of the truncated decahedron than the AOT molecules. The consequence is the large dominance of the lateral {100} facets compared to the top {111} facets. On the other hand, it can be speculated that the short elongated particles formed in the absence of salt are the precursors required for the growth of longer elongated particles. Whatever the exact process is, the selective adsorption of the chloride anion constitutes a key parameter in the formation of elongated nanocrystals with a large aspect ratio. As described above, the kinetic growth of the particle length with the anion concentration is characterized by a maximum, whereas the width regularly increases. This behavior could be attributed to a change of surface energy with particle size. At low Cl^- concentration, that is, for smaller particles, the anion preferentially adsorbs on the higher surface energy, that is, the {100} surface. Now, at higher Cl^- concentration, when the particle is large, the surface energies of the {111} and {100} facets could become similar, inducing the anion adsorption on all of the enclosed facets of the nanocrystal. If this hypothesis is right and if we consider that the AOT molecules play a role at this stage of the growth process, they are also expected to follow the same behavior.

We will now consider the behavior observed in the presence of sodium bromide. The addition of NaBr in the same concentration range as NaCl (see Appendix D) induces a population characterized by the same diversity of shapes as obtained previously, but in the present case, the cubes, instead of the elongated nanocrystals, constitute the highest shape weight percentage (Figure 14). Their average size is 40 nm. The elongated particle size does not drastically change with NaBr addition.

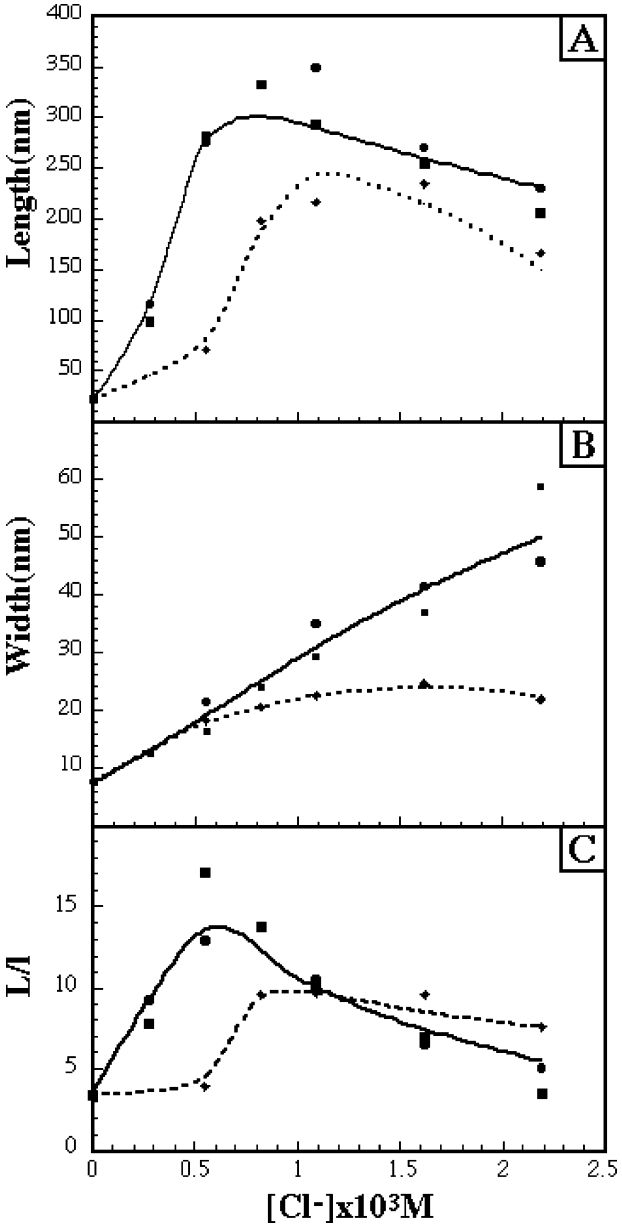

Figure 13. Variation of the length (A), the width (B), and the aspect ratio (C) with chloride concentration: (■) [NaCl]; (●) $CuCl_2$; (♦) CTAC.

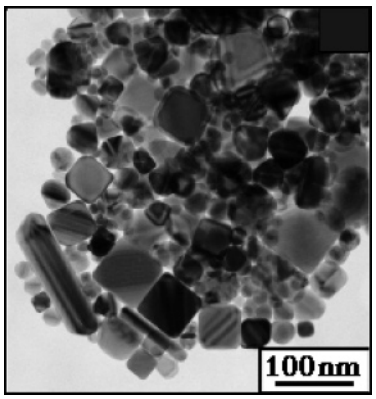

Figure 14. TEM patterns of nanocrystals obtained in the interconnected cylinder phase in the presence of sodium bromide. [NaBr] = 1.6×10^{-3} M.

The structural study of the cubes indicates that they have a cuboctahedral structure.[86] The HRTEM image of such a nanocrystal (Figure 15A) and the simulated image of a cubic cuboctahedral structure (Figure 15C) show two characteristic lattice planes perpendicular to each other, corresponding to a pure fcc structure. The calculated (Figure 15B) and simulated (Figure 15D) PS both confirm this structure. Reflections 1 and 2 correspond to the (200) ($d_1 = d_2 = d_{200} = d_{020} = 0.18$ nm) planes, and reflections 3 and 4 correspond to the (220) ($d_3 = d_4 = d_{200} = d_{2-20} = 0.127$ nm) planes. The (200) planes are perpendicular to each other as for the (220) planes. Thus, copper cubes are characterized by the cuboctahedron structure viewed along the [001] direction and are enclosed by the {100} surfaces. Their formation can be explained from the cuboctahedral precursor. As the typical facets of this precursor are the {100} and {111} ones, the cube growth is promoted by the specific growth of the {111} facets of the cuboctahedral precursor. This result is only made possible by the selective adsorption of the bromide anions on these facets that progressively disappears in favor of the {100} facets (Figure 15E).

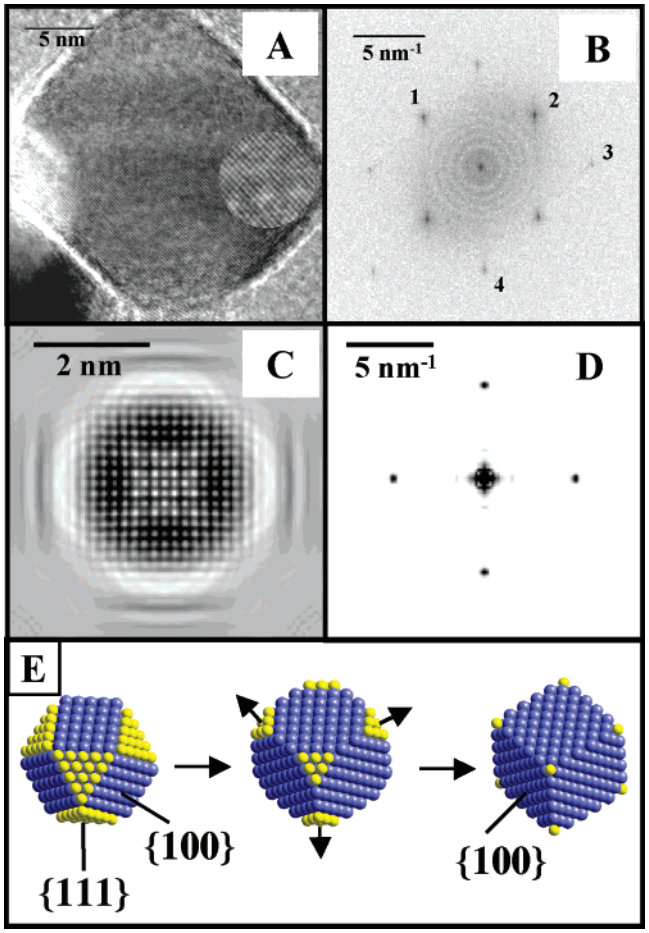

Figure 15. Cubic copper cuboctahedron nanocrystals in the [001] orientation produced at $R = 15$: (A) HRTEM image; (B) calculated power spectra; (C and D) computer simulations; (E) schematic of the growth mode of cubic nanocrystals.

Thus, the key parameters involved in the formation of cubic nanocrystals are both the presence of the cuboctahedral precursor and the selective adsorption of the bromide anion. It must be noted that the bromide anions do not change the elongated particle growth. This suggests that, for a given material, the ionic selective adsorption is a complex process not only related to the crystallographic nature of the surface but also related to the surface energies that vary with the precursor involved. Clearly, a given salt will not give rise to a specific particle shape; this fact is well illustrated in the literature. For example, cubic

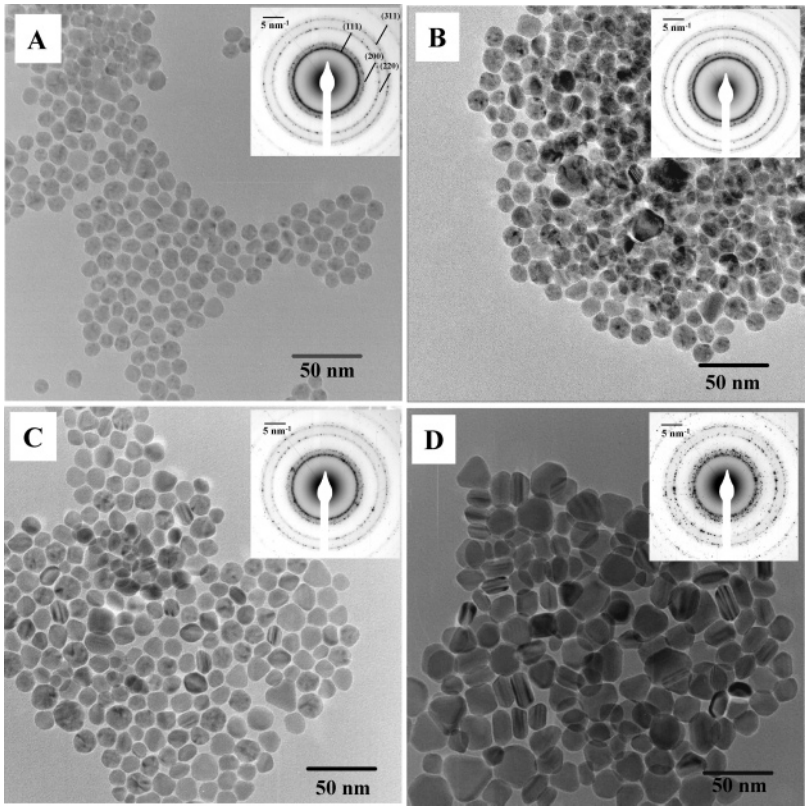

Figure 16. TEM patterns of copper nanocrystals obtained at various R values: (A) $R = 3$; (B) $R = 5$; (C) $R = 10$; (D) $R = 15$. The insets show the electron diffraction patterns corresponding to each sample in a collection of nanoparticles.

$KMnF_3$ nanocrystals are obtained by the use of the micelle technique, in the presence of bromide and chloride ions.[90] Cubic Pt nanocrystals are obtained by bubbling hydrogen through an aqueous solution containing $PtCl^{4-}$.[91] Gold nanorods are produced by ultraviolet−visible irradiation of a gold salt ($HAuCl_4$) solubilized in the bulk aqueous phase of normal micelles made of CTAC.[92]

V.3. Shape Control by Using Reverse Micelles in a Supersaturated Regime.[86] Another route to producing nonspherical nanocrystals is to use reverse micelles in a supersaturated regime. For instance, a set of syntheses of copper nanocrystals has been made in mixed AOT reverse micelles at higher and higher reducing agent concentrations (see Appendix E). Under these conditions, $R = [N_2H_4]/[Cu(AOT)_2]$, R varies from 3 to 15, whereas the water content, w, remains at 10. This means that, whatever the reducing agent concentration is, the chemical reduction takes place at the same polar volumic fraction. At low hydrazine concentration, $R = 3$, the population is mainly composed of "spherical" nanocrystals, including more or less regular spheres and pentagons, and their mean size is 12 nm (Figure 16A). Then, by progressively increasing R, the nanocrystals become more highly facetted with the appearance of new shapes (Figure 16B and C). At $R = 15$, copper atoms are implied in the formation of various shapes such as elongated nanocrystals, triangles, cubes, and "spheres" (Figure 16D). Their percentages are 31, 30, 9, and 30%, respectively. The average sizes are 23, 19, and 20 nm for the triangles, the cubes, and the spheres, whereas the elongated particles have an average length, width, and aspect ratio of 22 nm, 13 nm, and 1.8. It has to be noted that the R increase is also accompanied by the improvement of the particle crystallinity. This is partly illustrated by the formation of the nonspherical shapes; on the other hand, spherical particles also become more highly crystallized. It must be noted that, for any R value, electronic diffraction studies show no traces of copper oxide (insets of Figure 16). This fact is further confirmed by the HRTEM study of the various shapes (see below). These results are explained as follows: At $R = 3$, all the copper ions are not totally reduced. Hence, an increase in R induces the increase in the reduction yield, that is, the increase in the number of copper atoms, as observed previously (see section III.1). As the polar volume fraction remains unchanged, the precursor concentration increases, leading to larger nanocrystal sizes. As a second consequence of the high local concentrations of reageants, that is, of their high degree of confinement, particle crystallinity is improved. To illustrate the latter behavior, a careful structural study has been made of the various shape populations obtained at large R. The structures of the elongated and cubic nanocrystals are those described previously (see section V.2). They are characterized by the truncated decahedral and cuboctahedral structures, respectively. Their growth processes are related to the AOT molecule selective adsorption on the {100} facets. We will now focus on the other shapes consisting of triangles, pentagons, and spheres.

The HRTEM image (Figure 17A) shows a triangular nanocrystal, which exhibits three lattice planes, while the corresponding calculated PS (Figure 17B) shows four pairs of reflections labeled 1, 2, 3, and 4.[72,79] The lattice parameters are $d_1 = d_2 = d_3 = 0.221$ nm and $d_4 = 0.128$ nm. Reflections 1, 2, and 3 correspond to the forbidden 1/3{422} reflections related to the fcc structure. The angle between these planes is 60°. The observation of such reflections depends on the number of close-packed planes and the number of defects. Reflection 4 corresponds to the (220) planes of an fcc copper single crystal oriented in the [111] direction. The triangles appear to be flat particles with stacking faults and are characterized by an fcc structure oriented in the [111] direction. These objects are also called "trigonal lamellar particles". The precursors required for

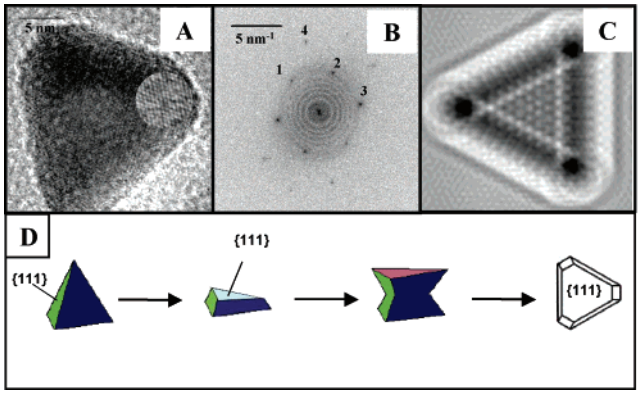

Figure 17. Triangular particle of copper oriented in the [111] direction: (A) HRTEM image; (B) calculated power spectrum; (C) computer simulation; (D) schematic of the growth mode of triangular copper nanocrystals.

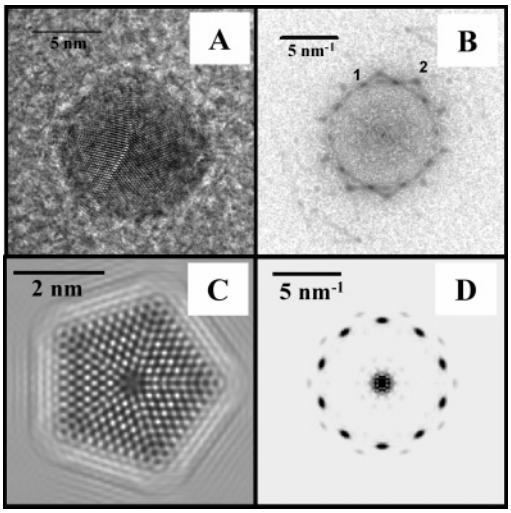

Figure 18. Copper decahedron oriented along the 5-fold axis, nanocrystals obtained at $R = 3$: (A) HRTEM image; (B) calculated power spectrum; (C and D) computer simulations.

their formation must contain a unique 3-fold axis, which is expressed in the final shape of the nanocrystal. Among the stable copper precursors, the decahedron, the cuboctahedron, and the tetrahedron, only the last can be modified simply to give rise to such a particle shape. Indeed, if a regular fcc tetrahedron is truncated on a {111} surface and then twinned by reflection at this surface, then a suitable precursor for the trigonal lamellar particle can be obtained (Figure 17D). Such a bitetrahedral precursor possesses the required 3-fold symmetry and, more importantly, contains three active sites for growth to maintain the overall 3-fold symmetry in the final nanocrystal. The truncation is attributed to the capping of AOT surfactant on one of the edges (as in the case related to the truncation of decahedra) and then on the subsequent {111} facets of the tetrahedral units.

The term "spheres" includes pentagonal and regular spherical shapes. At high *R* values, giving rise to more highly crystallized particles, these two shapes are related to regular decahedral (Figure 18) and cuboctahedral (Figure 19) nanocrystals. The HRTEM images of the nanocrystals (Figures 18A and 19A) are in good agreement with the simulated images of a decahedron viewed along the 5-fold orientation (Figure 18C) and a cuboctahedron viewed along the [111] orientation (Figure 19C). For the decahedron, the calculated PS is characterized by 10 pairs of reflections: 5 pairs labeled 1 ($d_1 = 0.208$ nm) and 5 others labeled 2 ($d_2 = 0.180$ nm) corresponding,

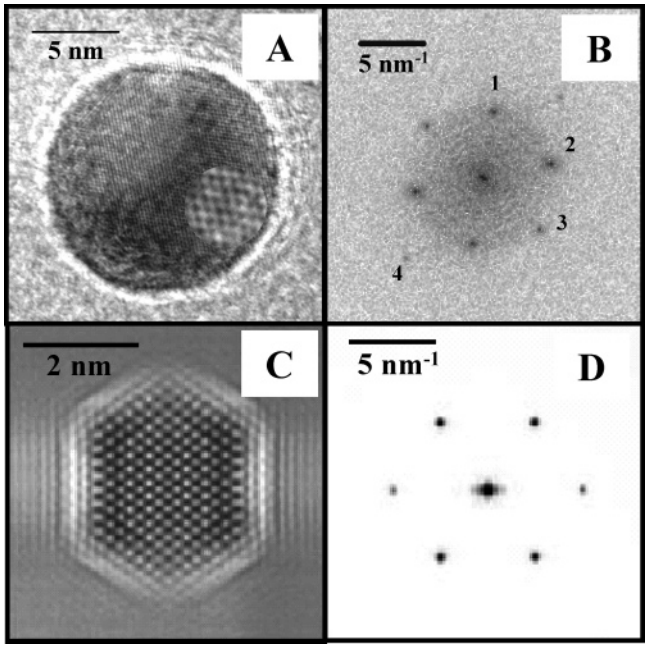

Figure 19. Spherical fcc copper nanocrystals in the [110] orientation produced at $R = 15$: (A) HRTEM image; (B) calculated power spectrum; (C and D) computer simulations.

respectively, to the (111) and (200) planes of the five fcc subunits (Figure 18B). The calculated PS (Figure 18B) is in good agreement with the simulation (Figure 18D). Therefore, pentagonal particles are decahedrons consisting of five deformed tetrahedral subunits twinned by their {111} planes and then characterized by a 5-fold symmetry. For the cuboctahedron, the calculated PS (Figure 19B) shows four pairs of reflections labeled 1, 2, 3, and 4 that correspond to the following lattice parameters: $d_1 = d_2 = 0.208$ nm, $d_3 = 0.180$ nm, and $d_4 = 0.127$ nm related to the (111), (200), and (220) planes, respectively, of an fcc structure. Thus, regular spherical particles have a cuboctahedral structure. Both these shapes are induced by the homogeneous growth of their precursors which are the decahedron and the cuboctahedron, respectively. No transformation such as facet truncation or preferential growth of facets is required. It can be assumed that, in these cases, the AOT surfactant homogeneously adsorbs on the enclosed facets of the crystal with a similar affinity. It has to be noted that, at an *R* value of 3, most of the "spherical" particles are characterized by many defects.

Such results are partially based on the improvement of the particle crystallinity induced by the supersaturated regime. Similar to the synthesis made in the interconnected cylinder phase (see section V.1), it seems that the confinement of the reagents constitutes a key parameter. Hence, at large *R*, the high particle crystallinity makes possible the growth of well-defined shapes. It clearly appears that the diversity of the particle morphologies (cube, triangle, pentagon, sphere, and elongated particle) is related to the various decahedral, cuboctahedral, and tetrahedral copper precursors. Moreover, as the AOT adsorption appears to be a versatile process, a given precursor can induce various growth processes. Therefore, when the surfactant adsorption is selective, triangles, cubes, and elongated particles form, whereas, the absence of surfactant selectivity gives rise to spheres and pentagons. Conversely to what is obtained in the interconnected cylinder phase in the presence of salt, no shape emerges preponderantly. This clearly shows that the selective adsorption of the AOT molecules compared to the salt as Cl^- and Br^- is much less. Some examples of supersaturated

regimes inducing the formation of nonspherical nanocrystals are given in the literature. Silver nanodisks are produced, in the presence of Na(AOT)/Ag(AOT) surfactant, that no longer form well-defined reverse micelles when the concentration of hydrazine used as the reducing agent is large.[29,30] Flat triangular CdS nanocrystals are obtained by using $Cd(AOT)_2$ reverse micelles saturated by H_2S.[28] In the same way, by bubbling H_2 through an aqueous solution containing $PtCl_4^-$, cubic platinum can be obtained.[91] For any reaction system, saturation with either the reducing agent or one of the reagents seems to be primary in the formation of well-crystallized nonspherical nanoparticles. Nevertheless, concerning the chemical reductions, the selective adsorption of the hydrazine on the crystal facets cannot be excluded.[94,95]

VI. Conclusion

In this paper, we provide evidence for the various key parameters involved in the control of the size, the structure, and the shape of metallic nanocrystals synthesized in colloidal assemblies. It clearly appears that AOT reverse micelles can be used either as nanoreactors or as simple stabilizing agents. With these, a collection of various spherical copper nanocrystal sizes (from 2.1 to 12.6 nm) is obtained. Magnetic cobalt nanocrystals (7.2 nm) are also produced, and their rather low size distribution makes possible their spontaneous organization in 2D compact hexagonal networks and in fcc supracrystals over a long range. Furthermore, we demonstrate that the best control of the particle shape is obtained by combining the strategy of the surfactant-based template and the selective adsorption of salts.

Acknowledgment. I would like to thank Professor J. Urban for providing the structural models.

Appendix A: Synthesis Procedures for Spherical Copper Nanocrystals

A1. Colloidal copper nanocrystals are obtained by mixing two solutions. The first is a mixed micellar solution containing 10^{-2} M $Cu(AOT)_2$. The overall AOT concentration is 0.1 M, and the oil is isooctane. The second contains the hydrazine used as the reducing agent. The ratio of hydrazine concentration to the $Cu(AOT)_2$ concentration is 3. The water content, w, changes from 1 to 15. The reaction takes place over 3 h.

The following synthesis procedures are based on that described in A1. Only the modifications are mentioned.

A2. The solvent is cyclohexane.

A3. Change in the polar volume fraction, Φ, as follows:

For $w = 3$, $0.8\% < \Phi < 3.2\%$. For $w = 10$, $3.2\% < \Phi < 9.6\%$.

A4. The overall AOT surfactant is 0.3 M, and the $Cu(AOT)_2$ surfactant concentration is changed as follows:

For $w = 3$ and 10, 0.25×10^{-2} M $< [CuAOT)_2] < 4 \times 10^{-2}$ M.

A5. Change in the overall AOT surfactant concentration as follows:

For $w = 3$, 0.4 M $<$ [AOT] $<$ 6 M. For $w = 10$, 0.8 M $<$ [AOT] $<$ 6 M.

Appendix B: Synthesis Procedure for Spherical Cobalt Nanocrystals

Cobalt nanocrystals are obtained by mixing two solutions. The first is a pure micellar solution containing cobalt ions as counterions. The overall AOT concentration is 0.1 M, the solvent is isooctane, and the water content is 32. The second contains sodium borohydride, $NaBH_4$, used as the reducing agent. The ratio of the $NaBH_4$ concentration to the cobalt AOT concentration, R, varies from 0.5 to 8. The reaction lasts only a few seconds. The nanocrystals are then coated with lauric acid molecules and extracted from reverse micelles or from the surfactant; finally, the nanocrystals thus coated are dispersed in hexane. To eliminate the larger size crystals formed when the synthesis takes place in a supersaturated regime, that is, for $R > 1$, the solution is centrifuged and only the smaller sizes are collected.

Appendix C: Synthesis Procedure for Nonspherical Copper Nanocrystals in Various Colloidal Assemblies in the Absence of Salt

Colloidal copper nanocrystals are obtained by reducing copper ions in the various microstructures of the ternary system isooctane/$Cu(AOT)_2$/water following procedure A1. The $Cu(AOT)_2$ and N_2H_4 concentrations are 5×10^{-2} and 0.15 M.

Appendix D: Synthesis Procedure for Elongated and Cubic Copper Nanocrystals in the Interconnected Cylinder Phase and in the Presence of Salt

Colloidal copper nanocrystals are obtained by reducing copper ions in the interconnected cylinder microreactor following procedure A1. The $Cu(AOT)_2$ and N_2H_4 concentrations are 5×10^{-2} and 0.15 M; $w = 9.5$.

When the salt is NaCl, $0 < [NaCl] < 2.5 \times 10^{-3}$ M.

When the salt is NaBr, $[NaBr] = 1.6 \times 10^{-3}$ M.

Appendix E: Synthesis Procedure for Various Shapes of Copper Nanocrystals in AOT Reverse Micelles in a Supersaturated Regime

Colloidal copper nanocrystals are obtained by mixing two solutions. The first is a mixed micellar solution containing 10^{-2} M $Cu(AOT)_2$. The overall AOT concentration is 0.1 M, and the solvent is isooctane. The second contains the hydrazine used as the reducing agent. The ratio of the hydrazine concentration to the $Cu(AOT)_2$ concentration, $R = [N_2H_4]/[Cu(AOT)_2]$, varies from 3 to 15. The water content, w, is kept constant at 10.

References and Notes

(1) Heath, J. R. *Acc. Chem. Res.* **1999**, *32*, 388.
(2) Vollat, V.; Szabo, D. V.; Taylor, R. D.; Willis, J. O. *J. Mater. Res.* **1997**, *12*, 2175.
(3) Perez, A.; et al. *Mater. Trans.* **2001**, *42*, 1460.
(4) Murray, C. B.; Norris, D. J.; Bawendi, M. G. *J. Am. Chem. Soc.* **1993**, *115*, 8706.
(5) Pileni, M. P. *J. Phys. Chem.* **1993**, *97*, 6961.
(6) Pileni, M. P. *Langmuir* **1997**, *13*, 3266.
(7) Pileni, M. P. *Langmuir* **2001**, *17*, 7476.
(8) Klabunde, K. J. *Nanoscale Materials in Chemistry*; Wiley-Interscience: New York, Chichester, Weinheim, Brisbane, Singapore, Toronto, 2001.
(9) Cepak, V. M.; Martin, C. R. *J. Phys. Chem.* **1998**, *102*, 9985.
(10) Molares, M. E. Toimil; Buschmann, V.; Dobrev, D.; Neumann, R.; Scholz, R.; Schuchert, I. U.; Vetter, J. *Adv. Mater.* **2001**, *13*, 62.
(11) Namatsu, H.; Kurihara, K.; Nagase, M.; Makino, T. *Appl. Phys. Lett.* **1997**, *70*, 619.
(12) Wang, J.; Thomson, D. A.; Robinson, B. J.; Simmons, J. G. *J. Cryst. Growth* **1997**, *175*, 793.
(13) Nepojko, S. A.; Levlev, D. N.; Schulze, W.; Urban, J.; Ertl, G. *ChemPhysChem* **2000**, 140.
(14) Yu. Y. Y.; Chang, S. S.; Lee, C. L.; Wang, C. R. *J. Phys. Chem. B* **1997**, *101*, 6661.
(15) Huang, L.; et al. *Adv. Mater.* **2002**, *14*, 61.
(16) Wang, Z. L.; Gao, R. P.; Nikoobakht, B.; El Sayed, M. *J. Phys. Chem. B* **2000**, *104*, 9985.

(17) Peng, X.; Manna, L.; Yang, W.; Wickham, J.; Sher, E.; Kadavanich, A.; Alivisatos, A. P. *Nature* **2000**, *404*, 59.
(18) Puntes, V. F.; Krishnan, K. M.; Alivisatos, A. P. *Science* **2001**, *291*, 2115.
(19) Cordente, N.; Respaud, M.; Senocq, Casanove, M. J.; Amiens, C.; Chaudret, B. *Nano Lett*. **2001**, *1*, 565.
(20) Dumestre, F.; Chaudret, B.; Amiens, C.; Fromen, M. C.; Casanove, M. J.; Renaud, P.; Zurcher, P. *Angew. Chem*. **2002**, *114*, 4462.
(21) Pileni, M. P. *Nat. Mater.* **2003**, *2*, 145
(22) Lisiecki, I. *Colloids Surf., A* **2004**, *250*, 499.
(23) Pileni, M. P. *Catal. Today* **2000**, *58*, 151.
(24) Lisiecki, I.; Pileni, M. P. *J. Am. Chem. Soc*. **1992**, *115*, 3887.
(25) Tanori, J.; Pileni, M. P. *Langmuir* **1997**, *13*, 639.
(26) Pileni, M. P.; Gulik-Krzywicki, T.; Tanori, J.; Filankembo, A.; Dedieu, J. C. *Langmuir* **1998**, *14*, 7359.
(27) Filankembo, A.; Giorgio, S.; Lisiecki, I.; Pileni, M. P. *J. Phys. Chem. B* **2003**, *107*, 7492.
(28) Pinna, N.; Weiss, K.; Urban, J.; Pileni, M. P. *Adv. Mater.* **2001**, *13*, 261.
(29) Maillard, M.; Giorgio, S.; Pileni, M. P. *Adv. Mater.* **2002**, *14*, 1084.
(30) Germain, V.; Li, J.; Ingert, D., Wang, Z. L.; Pileni, M. P. *J. Phys. Chem. B* **2003**, *107*, 34.
(31) Salzemann, C.; Lisiecki, I.; Urban, J.; Pileni, M. P. *Langmuir* **2004**, *20*, 11772.
(32) Motte, L.; Billoudet, F.; Pileni, M. P. *J. Phys. Chem*. **1995**, 16425.
(33) Murray, C. B.; Kagan, C. R.; Bawendi, M. G. *Science* **1995**, *270*, 1335.
(34) Motte, L.; Billoudet, F.; Lacaze, E.; Pileni, M. P. *Adv. Mater*. **1996**, *8*, 1018.
(35) Harfenist, S. A.; Wang, Z. L.; Alvarez, M. M.; Vezmar, I.; Whetten, R. L. *J. Phys. Chem.* **1996**, *100*, 13904.
(36) Taleb, A.; Petit, C.; Pileni, M. P. *Chem. Mater.* **1997**, *9*, 950.
(37) Harfenist, S. A.; Wang, Z. L.; Whetten, R. L.; Vezmar, I.; Alvarez, M. M. *Adv. Mater.* **1997**, *9*, 817.
(38) Ohara, P. C.; Heath, J. R.; Gelbart, W. M. *Angew. Chem., Int. Ed. Engl*. **1997**, *36*, 1078.
(39) Vijaya Sarathy, K.; Raina, G.; Yadav, R. T.; Kullkarni, G. U.; Rao, C. N. R. *J. Phys. Chem. B* **1997**, *101*, 9876.
(40) Taleb, A.; Petit, C.; Pileni, M. P. *J. Phys. Chem. B* **1998**, *102*, 2214.
(41) Korgel, B. A.; Fullam, S.; Connoly, S.; Fitzmaurice, D. *J. Phys. Chem*. **1998**, *102*, 8379.
(42) Petit, C.; Taleb, A.; Pileni, M. P. *Adv. Mater.* **1998**, *10*, 259.
(43) Petit, C.; Taleb, A.; Pileni, M. P. *J. Phys. Chem B* **1999**, *103*, 1805.
(44) Giersig, M.; Hilgendorff. *J. Phys. D* **1999**, *32*, L111.
(45) Murray, C. B, Sun, S.; Gaschler, W., Doyle, H.; Betley, T. A, Kagan, C. R. *IBM. J. Res. Dev*. **2001**, *45*, 47.
(46) Black, C. T.; Murray, C. B.; Sandstrom, R. L.; Sun, S. *Science* **2000**, *290*, 1131.
(47) Dumestre, F.; Martinez, S.; Zitoun, D.; Fromen, M. C.; Casanove, M. J.; Lecante, P.; Respaud, P.; Serres, A.; Benfield, R. E., Amiens, C.; Chaudret, B. *Faraday Discuss. Chem. Soc*. **2004**, *125*, 265.
(48) Pinna, N.; Maillard, M.; Courty, A.; Russier, V.; Pileni, M. P. *Phys. Rev. B* **2002**, *66*, 45415.
(49) Courty, A.; Mermet, A.; Albouy, P. A.; Duval, E.; Pileni, M. P. *Nat. Mat.*, submitted for publication.
(50) Russier, R.; Petit, C.; Legrand, J.; Pileni, M. P. *Phys. Rev. B* **2000**, *62*, 3910.
(51) Ngo, T.; Pileni, M. P. *Adv. Mater*. **2000**, *12*, 276.
(52) Russier, V. *J. Appl. Phys*. **2001**, *89*, 1287.
(53) Ngo, T.; Pileni, M. P. *J. Phys. Chem*. **2001**, *105*, 53.
(54) Pileni, M. P. *J. Phys. Chem. B* **2001**, *105*, 3358.
(55) Pileni, M. P. *Reactivity in Reverse Micelles*; Elsevier: Amsterdam New York, Oxford, Shannon, Tokyo, 1989.
(56) Mitchell, D.; Ninham, B. *J. Chem. Soc., Faraday Trans. 2* **1981**, *77*, 601.
(57) Pileni, M. P.; Zemb, T.; Petit, C. *Chem. Phys. Lett*. **1985**, *118*, 414.
(58) Cassin, G., Badiali, J. P.; Pileni, M. P. *J. Phys. Chem.* **1995**, *99*, 12941.
(59) Van Dijk, M. A. *Phys. Rev. Lett.* **1985**, *9*, 1003.
(60) Huang, J. S. *J. Chem. Phys.* **1985**, *82*, 480.
(61) Lemaire, B.; Bothorel, P.; Roux, D. *J. Phys. Chem.* **1983**, *87*, 1023.
(62) Huang, J. S.; Safran, S. A.; Kim, M. W.; Grest, G.; Kotlarchyk, M.; Quirke, N. *Phys. Rev. Lett.* **1984**, *53*, 592.
(63) Robinson, B. H.; Toprakcioglu, C; Dore, J. C.; Chieux, P *J. Chem. Soc., Faraday Trans. 1* **1984**, 80.
(64) Jain, T. K.; Cassin, G.; Badiali, J. P.; Pileni, M. P. *Langmuir* **1996**, *12*, 2408.
(65) Petit, C.; Lixon, P.; Pileni, M. P. *Langmuir* **1991**, *7*, 2620.
(66) Eastoe, J.; Fragneto, G.; Robinson, B. H.; Towey, T. F.; Heenan, R. K.; Leng, F. J. *J. Chem. Soc., Faraday Trans.* **1992**, *88*, 461.
(67) Eastoe, J.; Steytler, D. C.; Robinson, B. H.; Heenan, R. K.; North, A. N.; Dore, J. C. *J. Chem. Soc., Faraday Trans.* **1994**, *90*, 2479.
(68) Eastoe, J.; Robinson, B. H.; Heenan, R. K. *Langmuir* **1993**, *9*, 2820.
(69) Eastoe, J.; Towey, T. F.; Robinson, B. H.; Williams, J.; Heenan, R. K. *J. Phys. Chem.* **1993**, *97*, 1459.
(70) Tanori, J.; Gulik, T.; Pileni, M. P. *Langmuir* **1997**, *13*, 639.
(71) Lisiecki, I.; André, P.; Filankembo, A.; Petit, C.; Tanori, J.; Gulik-Krzywicki, T.; Ninham, B. W.; Pileni, M. P. *J. Phys. Chem*. **1999**, *103*, 9168.
(72) Lisiecki, I.; André, P.; Filankembo, A.; Petit, C.; Tanori, J.; Gulik-Krzywicki, T.; Ninham, B. W.; Pileni, M. P. *J. Phys. Chem*. **1999**, *103*, 9176.
(73) André, P.; Filankembo, A.; Lisiecki, I.; Petit, C.; Gulik- Krzywicki, T.; Ninham, B. W.; Pileni, M. P. *Adv. Mater*. **2000**, *12*, 119.
(74) André, P.; Ninham, B. W.; Pileni, M. P. *Adv. Colloid Interface Sci.* **2001**, *89*, 155.
(75) André, P.; Ninham, B. W.; Pileni, M. P. *New J. Chem*. **2001**, *25*, 563.
(76) Lisiecki, I.; Pileni, M. P. *J. Am. Chem. Soc*. **1993**, *115*, 3887.
(77) Lisiecki, I.; Pileni, M. P. *J. Phys. Chem*. **1995**, *99*, 5077.
(78) Petit, C.; Lixon, P.; Pileni, M. P. *J. Phys. Chem*. **1993**, *97*, 12974.
(79) Motte, L.; Lisiecki, I.; Pileni, M. P. In *Hydrogen Bond Networks*; Dore, J. C., Bellissent-Funel, M. C., Eds.; NATO publisher, 1994; p 447.
(80) Lisiecki, I.; Pileni, M. P. *Langmuir* **2003**, *19*, 9486.
(81) Lisiecki, I.; Albouy, P. A.; Pileni, M. P. *Adv. Mater*. **2000**, *15*, 119.
(82) Lisiecki, I.; Albouy, P. A.; Pileni, M. P. *J. Phys. Chem*., in press.
(83) Legrand, J.; Petit C.; Pileni, M. P. *J. Phys. Chem. B* **2001**, *105*, 5643.
(84) Legrand, J.; Petit, C.; Bazin, D. D.; Pileni, M. P. *Appl. Surf. Sci.* **2000**, *164*, 193.
(85) Lisiecki, I.; Filankembo, A.; Sack-Kongehl, H.; Weiss, K.; Pileni, M. P.; Urban, J. *Phys. Rev. B* **2000**, *61*, 4968.
(86) Salzemann, C.; Lisiecki, I.; Urban, J.; Pileni, M. P. *Langmuir*, in press.
(87) Simmons, B.; Li, S.; Jhon, V.; McPherson, G.; Bose, A.; Zhou, W.; He, J. *Nano Lett.* **2002**, *2*, 263.
(88) Wang, S.; Yang, S. *Langmuir* **2000**, *16*, 389.
(89) Filankembo, A.; Pileni, M. P. *J. Phys. Chem. B* **2000**, *104*, 5865.
(90) Agnoli, F.; Zhou, W. L.; O'Connor, C. J. *Adv. Mater*. **2001**, *13*, 1697.
(91) Heiglein, A.; Giersig, M. *J. Phys. Chem. B* **2000**, *104*, 6767.
(92) Esumi, K.; Matsuhisa, K.; Torigoe, K. *Langmuir* **1995**, *11*, 3285.
(93) Salzemann, C.; Urban, J.; Lisiecki, I.; Pileni, M. P. Submitted for publication.
(94) Li, Y.; Liao, H.; Ding, Y.; Fan, Y.; Zhang, Y.; Qian, Y. *Inorg. Chem.* **1999**, *38*, 1382.
(95) Li, Y.; Ding, Y.; Wang, Z. *Adv. Mater*. **1999**, *11*, 847.